ACS APPLIED MATERIALS & INTERFACES

Research Article

www.acsami.org

# Graphene-Wrapped Polyaniline Hollow Spheres As Novel Hybrid Electrode Materials for Supercapacitor Applications

Wei Fan,[†] Chao Zhang,[†] Weng Weei Tjiu,[‡] Kumari Pallathadka Pramoda,[‡] Chaobin He,[‡] and Tianxi Liu*,[†]

[†]State Key Laboratory of Molecular Engineering of Polymers, Department of Macromolecular Science, Fudan University, 220 Handan Road, Shanghai 200433, P. R. China

[‡]Institute of Materials Research and Engineering, A*STAR (Agency for Science, Technology and Research), 3 Research Link, Singapore 117602, Singapore

Supporting Information

**ABSTRACT:** Polyaniline hollow spheres (PANI-HS)@electrochemical reduced graphene oxide (ERGO) hybrids with core−shell structures have been fabricated *via* a solution-based coassembly process. The hollow nanostructured designing for the PANI-HS greatly enlarges the specific surface area, providing high electroactive regions and short diffusion lengths for both charge and ion transport. The wrapping of ERGO sheets on the PANI-HS can offer highly conductive pathways by bridging individual PANI-HS together, thus facilitating the rate and cycling performance of supercapacitors. The specific capacitance of PANI-HS36@ERGO hybrids can reach 614 F $g^{-1}$ at a current density of 1 A $g^{-1}$. Furthermore, the capacitance of the PANI-HS36@ERGO hybrids maintains 90% after 500 charging/discharging cycles at a current density of 1 A $g^{-1}$, indicating a good cycling stability. The greatly enhanced electrochemical performance can be ascribed to the synergic effects of the two components of PANI-HS and ERGO, suggesting that the PANI-HS@ERGO hybrids as novel electrode materials may have potential applications in high-performance energy storage devices.

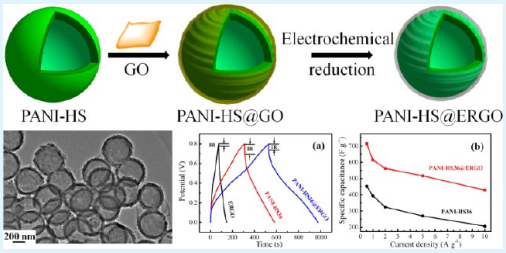


**KEYWORDS:** *graphene, polyaniline hollow spheres, hollow nanostructures, hybrid, supercapacitors, electrochemical properties*

## 1. INTRODUCTION

Electrochemical capacitors, which are also known as supercapacitors, are electrochemical energy storage devices with unique properties, such as high power, long cyclic life, fast charge−discharge rates, and low maintenance cost.[1,2] Supercapacitors have two energy storage mechanisms, namely, electrical double layer (EDL) capacitances and pseudocapacitances.[3,4] EDL capacitors, which can electrostatically store charges *via* reversible ion absorption at the electrode/electrolyte interface, commonly use carbon-based active materials with large surface areas and good electrical conductivity.[5] Carbon materials such as activated carbon (AC), mesoporous carbon (MC), and carbon nanotubes (CNTs) usually display good stability; however, their capacitance values are generally limited by the microstructures.[6] On the other hand, the pseudocapacitors or so-called redox supercapacitors undergo fast and reversible Faradaic redox reaction at the surfaces of electroactive materials that store the charges.[7] The large specific pseudocapacitance of Faradaic electrodes exceeds that of carbon-based materials using double-layer charge storage. Typical active pseudocapacitive materials include transition metal oxides, such as $RuO_2$, $MnO_2$, $Fe_3O_4$, NiO, and conducting redox polymers such as polyanilines (PANI), polypyrroles, and polythiophenes. However, they often exhibit poor stabilities during the charge/discharge processes, and the typical response times of pseudocapacitors are significantly longer than those of EDL capacitors.[8,9] Therefore, in order to further enhance the specific capacitance and cycle lives of supercapacitors, the pseudocapacitance can be coupled with the EDL capacitance by the immobilization of carbon materials with low-cost pseudocapacitive conducting polymers or metal oxides. This allows the systems to benefit from the synergetic merits of both EDL capacitance and pseudocapacitance, resulting in supercapacitors with high performance.

Recently, graphene has attracted much attention and been proved to be an outstanding candidate for electrode materials.[10−12] Graphene sheets are basically a 2D hexagonal lattice of $sp^2$ carbon atoms covalently bonded along two plane directions. Graphene exhibits exceptionally excellent thermal conductivity, electrical conductivity, mechanical properties, and high specific surface areas up to 2675 $m^2/g$.[13−15] More significantly, the intrinsic capacitance of graphene was recently found to be 21 $\mu F/cm^2$,[12] which sets the upper limit of EDL capacitance for all carbon-based materials and asserts that graphene is an ideal carbon electrode material for EDL

Received: February 1, 2013
Accepted: March 21, 2013
Published: March 21, 2013

  

supercapacitors. Thus, it is desirable to harness the unique properties of graphene and its derivatives in composites through the incorporation of various kinds of functional materials. Therefore, the potential usage of graphene-based materials for supercapacitors has attracted much attention recently.[16,17]

Among the various kinds of conducting redox polymers, PANI is considered as the most promising electrode material for supercapacitors, due to its excellent capacity for energy storage, easy synthesis, high conductivity, and low cost.[18−20] By the combination of the intriguing properties of graphene with those of PANI, hybrids of graphene and PANI have offered great promise as supercapacitors electrode materials, due to high conductivity, high surface area, and ability to store energy *via* two charge storage mechanisms. Recently, some efforts have been made on the incorporation of graphene into the PANI matrix to produce nanohybrids for supercapacitor electrodes.[18−37] However, most of the hybrids were fabricated by in situ polymerization of aniline in the presence of graphene oxide (GO) or chemically reduced graphene oxide (RGO),[19−22,35−37] and the PANI is in the forms of spheres,[21,34] nanowires,[18] nanofibers,[19,20,22] or nanorods.[33] Most recently, PANI/graphene composites with more complicated structures such as three-dimensional porous structures[38] and hydrogel films[39] have also been reported. Composites with these hierarchical nanostructures exhibit much more enhanced supercapacitor performance owing to their high surface area and low electrolyte transport resistance. However, to our knowledge, the research work on the hollow structured PANI/graphene hybrids has not been reported so far.

Hollow micro/nanostructured materials have been recognized as one type of promising material with numerous applications in energy-related fields.[40] The unique nanostructures, like porous or hollow structures, provide particular advantages to supercapacitors due to the enhanced surface-to-volume ratio and reduced transport lengths for both mass and charge transport.[41−44] In this study, we report the fabrication of polyaniline hollow spheres@electrochemical reduced graphene oxide (PANI-HS@ERGO) hybrids using a solution-based coassembly method. The PANI-HS was first synthesized by utilizing polystyrene (PS) spheres as hard templates. The resultant PANI-HS was positively charged in their emeraldine salt form, and subsequently the negatively charged GO sheets can wrap onto the PANI-HS *via* electrostatic interactions. The wrapped GO was finally reduced to ERGO by electrochemical reduction, leading to the final PANI-HS@ERGO hybrids. The as-prepared electroactive hybrid materials possess a porous structure for electrolyte access, which enhances the specific capacitance and the energy density of the electrodes. The specific capacitance of PANI-HS@ERGO hybrids reaches as high as 614 F $g^{-1}$, at a current density of 1 A $g^{-1}$. This value is substantially larger than those reported for graphene-PANI-based supercapacitors, suggesting that the PANI-HS@ERGO hybrid electrode materials may have great potential applications in high-performance energy storage devices.

## 2. EXPERIMENTAL SECTION

**2.1. Materials.** Natural graphite powder (325 meshes) was purchased from Alfa-Aesar. Aniline and styrene were purchased from Sigma-Aldrich. Potassium persulfate (KPS), ammonium persulfate (APS), tetrahydrofuran (THF), ethanol, 98% $H_2SO_4$, 30% $H_2O_2$, $KMnO_4$, $NaNO_3$, and 37% HCl were supplied by China Medicine Co. Aniline and styrene were purified by distillation, and other reagents were used as received without further treatment. Deionized (DI) water was used throughout all the experiments.

**2.2. Preparation of PANI-HS.** Monodispersed PS spheres with diameters of 330 nm and 2.4 $\mu$m, respectively, were synthesized according to the procedures reported elsewhere.[45] Then, 0.30 g as-prepared PS spheres were dispersed in 30 mL of concentrated sulfuric acid, and the sulfonation reaction was allowed to take place at 40 °C for 6 h under stirring. After the centrifugation and washing processes, 0.26 g of sulfonated PS was obtained and then dispersed in 30 mL of DI water. Subsequently, different amounts of aniline monomer (5 wt %, 10 wt %, and 20 wt % relative to sulfonated PS) in 1 M HCl solution was added to the above solution under stirring in an ice bath. An aqueous solution of APS (5 mL, 1:1 molar ratio of APS to aniline) was added, and the reaction was allowed to proceed for 24 h at 0 °C. The PS@PANI spheres were collected by repeatedly centrifuging and washing with ethanol and water, respectively. After that, the PS cores were removed by dispersing the PS@PANI spheres in THF and stirring for 6 h at room temperature. Finally, the PANI-HS were collected by repeatedly centrifuging and washing with THF, followed by drying under vacuum at 40 °C for 12 h. PANI-HS with a shell of different thicknesses (i.e., 20 nm, 36 nm, and 80 nm) were denoted as PANI-HS20, PANI-HS36, and PANI-HS80, respectively.

**2.3. Preparation of PANI-HS@GO Hybrids.** Graphite oxide was synthesized by Hummers method[46] and exfoliated to give a brown dispersion of GO under ultrasonication. PANI-HS was diluted to 1 mg $mL^{-1}$ with DI water under sonication for 0.5 h. Then, 10 mL of GO suspension (0.5 mg $mL^{-1}$) was added to 50 mL of PANI-HS suspension, and the resulting mixture was sonicated for another 2 h. The mass ratio of GO to PANI-HS in the resultant hybrids was calculated to be 1:10. After repeatedly centrifuging and washing with ethanol and water, the resultant product was collected and dried under vacuum at 40 °C for 12 h.

**2.4. Electrochemical Reduction of PANI-HS@GO Hybrids.** A glassy carbon electrode (GCE, diameter 3 mm) was used as the substrate to prepare the hybrid samples modified electrode. GCE was carefully polished with alumina powders (0.3 and 0.05 $\mu$m) on a polishing cloth, rinsed thoroughly with DI water between each polishing step, sonicated in ethanol and water, and then allowed to dry at room temperature. The working electrode was prepared by casting the hybrid sample onto the GCE surface. Typically, 10 $\mu$L of the dispersion of PANI-HS@GO hybrids with a concentration of 1.0 mg $mL^{-1}$ was dripped onto the GCE surface and then naturally dried at room temperature to form the hybrid sample adsorbed GCE. The electrochemical reduction of the PANI-HS@GO hybrids on GCE was performed on the electrochemical workstation at a scan rate of 50 mV $s^{-1}$ in 0.2 M pH = 7.0 PBS solution.

**2.5. Characterization.** FTIR spectra were recorded with a 4 $cm^{-1}$ spectral resolution on a Nicolet Nexus 470 spectrometer equipped with a DTGS detector. Transmission electron microscopy (TEM) observation was performed with a JEOL 2100 TEM under an accelerating voltage of 200 kV. Scanning electron microscopy (SEM) characterization was conducted with a TS 5136MM scanning electron microscope at an accelerating voltage of 20 kV. The surface charge of synthesized PANI-HS and GO sheets was measured using a $\zeta$-potential analyzer (Malvern, Zetasizer nanozs). X-ray diffraction (XRD) patterns of the samples were conducted on an X'Pert Pro X-ray diffractometer with Cu $K_\alpha$ radiation ($\lambda$ = 0.1542 nm) under a voltage of 40 kV and a current of 40 mA. Raman spectra were measured on LabRam-1B French Dilor Com ($\lambda_{ex}$ = 632.8 nm). The Brunauer−Emmett−Teller (BET) surface area was measured using a Belsorp-max surface area detecting instrument by $N_2$ physisorption at 77 K.

**2.6. Electrochemical Measurements.** The electrochemical tests were carried out in 1 M $H_2SO_4$ aqueous electrolyte solution at room temperature. A three-electrode system was used, consisting of the sample modified GCE as the working electrode, platinum as the counter electrode, and Ag/AgCl electrode as the reference electrode. Cyclic voltammetry (CV), galvanostatic charge/discharge curves, and electrochemical impedance spectroscopy (EIS) were performed with a CHI 660C electrochemical workstation (Chenhua Instruments Co.,

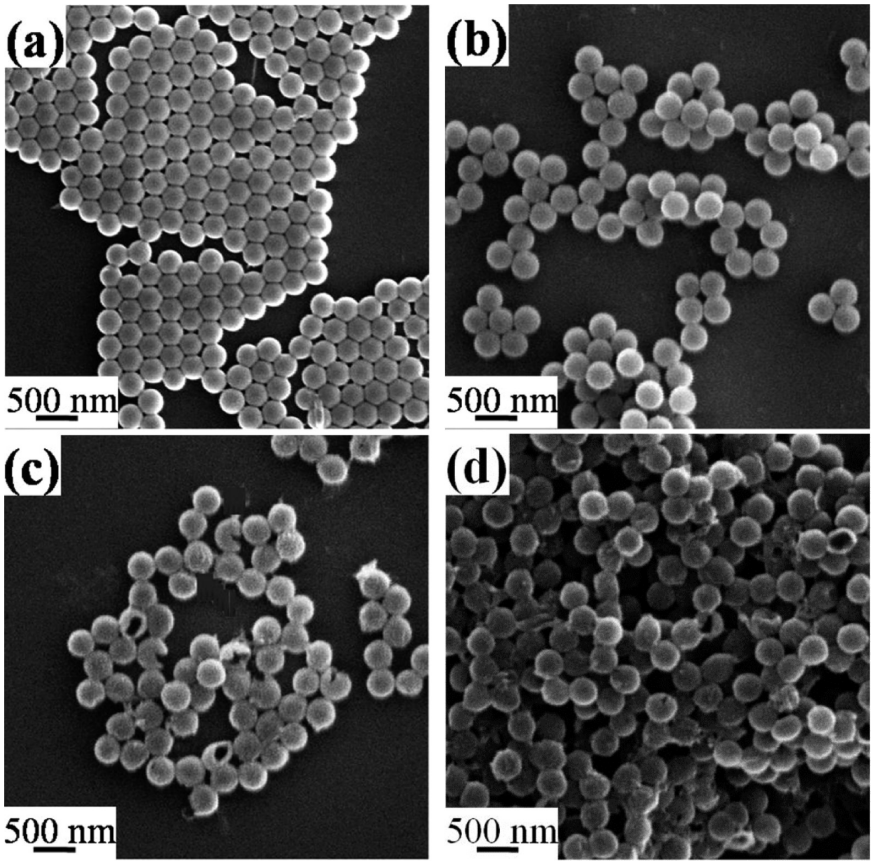


**Figure 1.** SEM images of (a) sulfonated PS, (b) PS@PANI, (c) PANI-HS36, and (d) PANI-HS36@GO hybrids.

Shanghai, China). CV curves were collected at different scan rates in a range from −0.2 to 0.8 V, and galvanostatic charge/discharge curves were measured in a voltage ranging from 0 to 0.80 V. EIS was recorded in the frequency range from $10^5$ to 0.01 Hz at open circuit potential with an alternating current (ac) voltage amplitude of 5 mV.

## 3. RESULTS AND DISCUSSION

**3.1. Morphology and Structure of PANI-HS@GO Hybrids.** Figure 1 shows the SEM images of sulfonated PS spheres, PS@PANI, PANI-HS36, and PANI-HS36@GO hybrids. The sulfonated PS spheres were prepared by an inward sulfonation from the surface of PS spheres. It was observed that these sulfonated PS spheres were uniform in size with an average diameter of 330 nm. The sulfonation of PS spheres is very important for the synthesis of PANI-HS hybrids, and the shell thickness of spheres is determined by the sulfonation time and temperature.[47] Typically, PS spheres were sulfonated with concentrated sulfuric acid at 40 °C for 6 h in this work. The sulfonation is verified by the FTIR spectrum. As shown in Figure S1 (Supporting Information), compared with PS spheres, the additional peaks at 1209 and 1006 $cm^{-1}$ are due to the sulfuric acid groups ($-SO_3H$) on the surface of sulfonated PS spheres.[48] Aniline can be adsorbed on the surface of sulfonated PS spheres and further in situ polymerized on the PS sphere surface when the oxidant is added, resulting in the formation of PS@PANI spheres (Figure 1b). The PANI-HS were produced by exposing the PS@PANI spheres to THF. The whole preparation process was illustrated in Scheme 1. It can be seen from Figure 1c that the PS cores were successfully removed. Some broken microspheres are observed in the SEM image, which clearly indicates they are hollow. This is further proven by the sharp contrast between the dark edge or shell and the pale center (or hollow core) of the hollow spheres in the TEM image (Figure 2b). The average thickness of the PANI layer is estimated to be about 36 nm. The PANI residues duplicated the original template structure very well and they were not out of shape due to the high strength of PANI shells.

**Scheme 1. Schematic Illustration of the Preparation of PANI-HS@ERGO Hybrids**

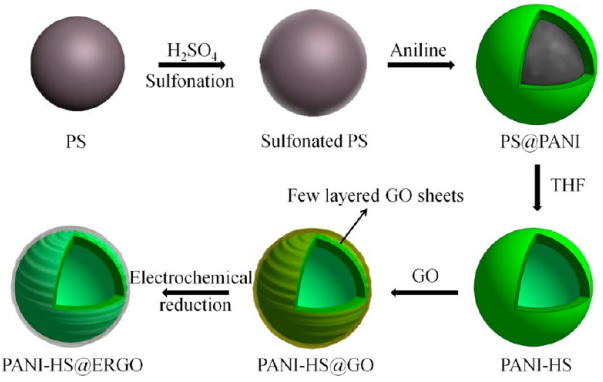


Graphite oxide was synthesized by Hummers method and exfoliated to give a brown dispersion of GO under sonication. The as-obtained GO suspension was intrinsically negatively charged due to the introduction of functional groups such as carboxylic acids (−COOH) on the surface of graphene sheets. The as-formed PANI-HS was proved to be positively charged in their emeraldine salt form. As determined by ζ-potential measurements, the ζ-potential values of the two dispersions are

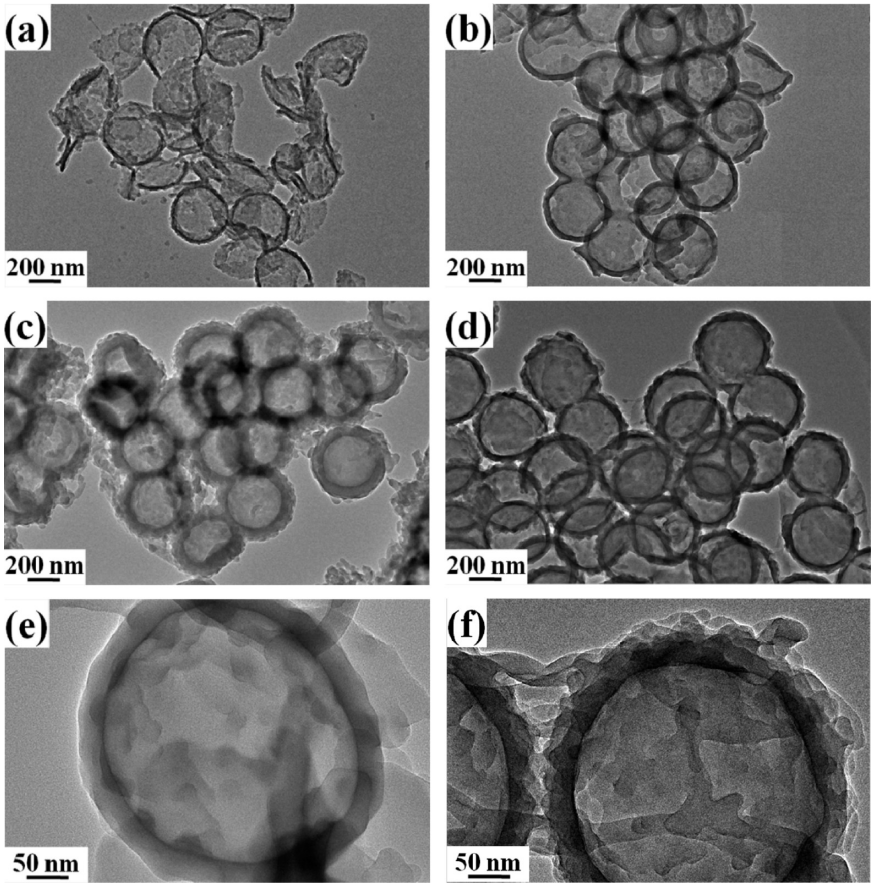


**Figure 2.** TEM images of (a) PANI-HS20, (b) PANI-HS36, (c) PANI-HS80, and (d) PANI-HS36@GO hybrids. Parts e and f show the corresponding TEM images of parts b and d at high magnifications.

+33 mV for PANI-HS and −50 mV for GO, respectively. PANI-HS@GO hybrids were synthesized by mixing the dispersion of PANI-HS and a controlled amount of GO under sonication in water, and the mixture coprecipitated immediately once the two dispersions were mixed. GO will assemble onto the surface of PANI-HS via multiple interactions, such as electrostatic, hydrogen bonding, and $\pi-\pi$ interactions, and subsequently GO wrapped PANI-HS hybrids were formed. As seen from the TEM image in Figure 2d, the smooth surface of the original PANI-HS became rough and some ribbon or sheet like features can be found between adjacent hollow spheres. In addition, an enlarged TEM image of an individual sphere obtained at a high magnification (Figure 2f) clearly shows the core−shell structure of the GO wrapped PANI-HS. Moreover, folding of GO sheets can be observed between the connected spheres, which prove that GO indeed wraps around the PANI-HS. The designed hollow nanostructure of the PANI-HS@GO hybrids can greatly enlarge the specific surface area. As shown in Figure S2 (Supporting Information), BET specific surface area of the PANI-HS@GO hybrids was further investigated by nitrogen isothermal adsorption. The isotherm curve belongs to the type IV with a clear hysteresis loop, which indicates that the PANI-HS@GO hybrids possess some mesoporous structures. The specific surface area of PANI-HS@GO hybrids was calculated to be 231 $m^2\ g^{-1}$, which is much higher than that of PANI nanospheres (79.3 $m^2\ g^{-1}$) as reported previously.[49]

Figure 3 shows the XRD patterns of GO, PANI-HS36, and PANI-HS36@GO hybrids. GO shows a typical diffraction peak

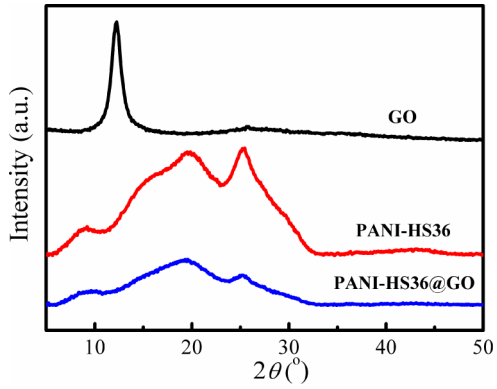


**Figure 3.** XRD patterns of GO, PANI-HS36, and PANI-HS36@GO hybrids.

at $2\theta$ = 10.6° as a result of the introduction of oxygenated functional groups on carbon sheets. For PANI-HS36, the reflection peaks appear at $2\theta$ = 19.4° and 25.2°, corresponding to (020) and (200) crystal planes of PANI in its emeraldine salt form, respectively.[50] The XRD data of PANI-HS36@GO hybrids present crystalline peaks similar to those obtained from pure PANI-HS36, revealing that no additional crystalline order has been introduced into the hybrids. Whereas, the diffraction peaks at $2\theta$ = 10.6° cannot be observed, indicating that GO sheets are fully interacted with PANI-HS36 and completely covered on PANI-HS36.


dx.doi.org/10.1021/am4003827 | ACS Appl. Mater. Interfaces 2013, 5, 3382−3391

Electrochemical reduction of PANI-HS36@GO hybrids was performed on GCE in a potential range from 0.0 to −1.5 V at different cathodic potentials in PBS solution. The cyclic voltammograms (Figure 4) show a large cathodic current

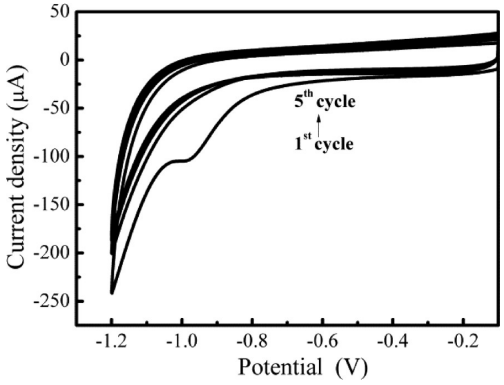


**Figure 4.** CV curves of PANI-HS36@GO hybrids at a scan rate of 50 mV $s^{-1}$ in 0.2 M PBS (pH = 7).

peak at −1.0 V with a starting potential of −0.75 V. This large reduction current should be due to the reduction of the surface oxygen groups since the reduction of water to hydrogen occurs at more negative potentials (e.g., −1.5 V).[51,52] Interestingly, the reduction peak was only produced during the first cycle of scanning and disappeared completely in the next cycles. This demonstrates that the reduction of surface-oxygenated species at GO occurs quickly and irreversibly, and GO can be reduced electrochemically at negative potentials. Therefore, after the first cycle of scanning, GO was reduced, that is, PANI-HS36@ERGO hybrids were obtained. In addition, the reduction of GO is also confirmed by Raman spectra. As shown in Figure S3 (Supporting Information), GO displays two prominent peaks at 1340 and 1597 $cm^{-1}$, corresponding to the well-documented D and G bands, respectively.[51] Although the Raman spectrum of ERGO also has both D and G bands, the intensity ratio of D/G increases obviously compared with that of GO, indicating the realization of deoxygenation upon reduction.[53] For the Raman spectrum of the PANI-HS36@ERGO hybrid, apart from the D and G bands of ERGO, three new representative peaks arising from PANI can be observed at 1165, 1240, and 1492 $cm^{-1}$, which correspond to in-plane C−H bending, C−N stretching vibration of the benzenoid ring, and C═N stretching of the quinoid.[26,30] However, compared with the spectrum of ERGO, the intensity ratio of the G to D bands in the PANI-HS36@ERGO hybrid increases. This finding demonstrates the influence of PANI on graphene due to the intimate interaction between them, which is consistent with previous results.[30]

**3.2. Electrochemical Behavior of PANI-HS@ERGO Hybrids.** The potential of using these hybrids as electrode materials for supercapacitors was tested by standard cyclic voltammetry (CV) and galvanostatic charge−discharge technique. Figure 5a illustrates the CVs of ERGO, PANI-HS36, and PANI-HS36@ERGO hybrids at a scan rate of 10 mV $s^{-1}$ in 1 M $H_2SO_4$ solution in the potential range from −0.2 to 0.8 V. The curves of ERGO electrodes exhibit an approximately rectangular shape which is characteristic of an EDL capacitor. Different from ERGO electrodes, both the PANI-HS36 and PANI-HS36@ERGO hybrid electrodes exhibit two pairs of redox waves which are an indication of a typical pseudocapacitive characteristic of PANI, corresponding to redox transitions

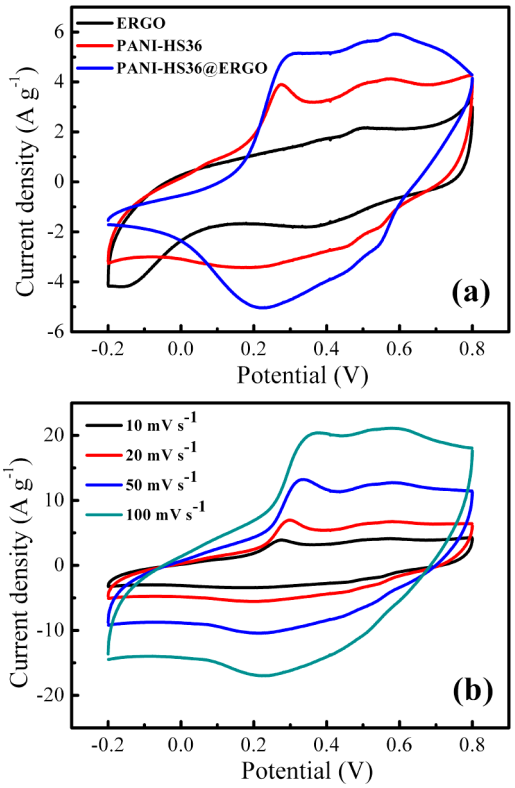


**Figure 5.** (a) CV curves of ERGO, PANI-HS36, and PANI-HS36@ERGO hybrids at a scan rate of 10 mV $s^{-1}$ in 1 M $H_2SO_4$ solution. (b) CV curves of PANI-HS36@ERGO hybrids at different scan rates of 10, 20, 50, and 100 mV $s^{-1}$, respectively.

of leucoemeraldine form (semiconductor)/polaronic emeraldine form (conductor) and Faradaic transformation of emeraldine/pernigraniline.[19,20] The CV curves of the PANI-HS36@ERGO hybrid electrode presents the behavior of a combination of both redox and EDL capacitance. It can be apparently found that the area of surrounded CV loops of PANI-HS36@ERGO hybrids is apparently larger than that of PANI-HS36, indicating a higher specific capacitance. The high capacitance is obviously ascribed to its unique structural features with high surface area, hierarchically porous structure, and thin shell thickness. The hollow-structured nanosized PANI spheres provide an enhanced electrode/electrolyte interface area, providing high electroactive regions and short diffusion lengths,[22] which can ensure a high utilization of PANI. Furthermore, ERGO in the hybrids can offer highly conductive pathways by bridging the adjacent individual PANI-HS together, thus facilitating rapid transport of the electrolyte ions in the electrode during rapid charge−discharge processes.[41] Therefore, the hybrids can greatly reduce the diffusion length, resulting in the improvement of electrochemical properties of PANI-HS36@ERGO hybrids. Meanwhile, it is worth mentioning that the specific capacitance of the PANI-HS36@GO hybrids is lower than that of pure PANI-HS36, as indicated from the CV curves in Figure S4 (Supporting Information). This is mainly due to the insulating nature of GO sheets in the hybrids, and the total capacitance is mainly dominated by the pseudocapacitance from the conducting PANI-HS.

Figure 5b shows the CV curves of PANI-HS36@ERGO hybrids at different scan rates. It is notable that the synthesized materials exhibit excellent electrochemical behavior in a wide

range of scan rates. It can be also observed that the oxidation peaks shift positively and the reduction peaks shift negatively with increasing potential sweep rates, which is mainly due to the resistance of the electrode.[54] Between 10 and 100 mV $s^{-1}$, the scan rate dependence of the peak current was investigated on the first redox waves of PANI. The peak currents evolve linearly with the square root of the scan rates, indicating a diffusion limited redox process.[55] In addition, the obvious increase of peak current density with the scan rates indicates a good rate ability for the PANI-HS36@ERGO hybrid electrode.

The representative charge−discharge curves at a current density of 1 A $g^{-1}$ are shown in Figure 6a. The specific

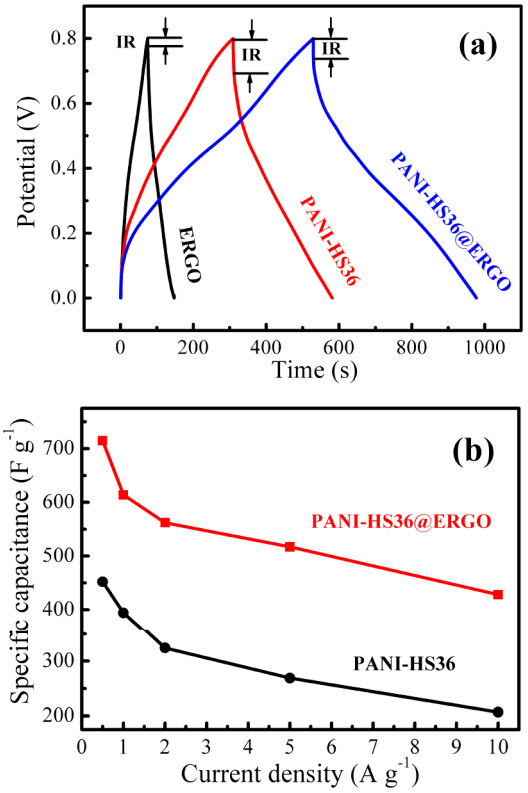


**Figure 6.** (a) Galvanostatic charge−discharge curves of ERGO, PANI-HS36, and PANI-HS36@ERGO hybrids within a potential window of 0−0.80 V at a current density of 1 A $g^{-1}$. (b) Plots of specific capacitance for PANI-HS36 and PANI-HS36@ERGO hybrids at various current densities.

capacitance $C$ (F $g^{-1}$) of the samples was estimated from the discharge process according to the following equation:

$$C = \frac{I\Delta t}{\Delta V \times m} \quad (1)$$

where $I$ is the current loaded (A), $\Delta t$ is the discharge time (s), $\Delta V$ is the potential change during discharge process, and $m$ is the mass of active material in a single electrode (g).

The ERGO electrode shows a triangular-shape charge−discharge curve, implying that its capacitance is mainly attributed to pure EDL capacitance. On the contrary, the discharging curve of PANI-HS36@ERGO hybrid electrode shows two voltage stages in the ranges of 0.8−0.45 V and 0.45−0 V, respectively. The first stage with a relatively short discharging duration is ascribed to pure EDL capacitance. However, the second stage with a much longer discharging duration is associated with a combination of EDL and Faradaic capacitances of the PANI-HS component.[56] Although the charge−discharge curves of PANI-HS36 maintain the similar shape of the PANI-HS36@ERGO hybrids, the "IR drop" of the PANI-HS36 electrode is much higher than that of the PANI-HS36@ERGO hybrid electrode, reflecting that the internal resistance of PANI is much higher than that of the hybrid. Low internal resistance is of great importance in energy storage devices, since less energy will be wasted to produce unwanted heat during charge−discharge processes.[22] PANI in its leucoemeraldine or pernigraniline form is an insulator; thus, the supercapacitor based on PANI-HS has a large internal resistance as it is fully charged or discharged. By forming a conductive network between the adjacent PANI-HS, ERGO greatly enhances the electronic conductivity of the hybrids, resulting in a low internal resistance. Thus, PANI-HS@ERGO hybrids are more suitable for fabricating safe and power saving supercapacitors.

Specific capacitances of ERGO, PANI-HS36, and PANI-HS36@ERGO hybrids were 93, 394, 614 F $g^{-1}$, respectively, which were estimated from the discharge process at a current density of 1 A $g^{-1}$. The excellent specific capacitive ability of the PANI-HS36@ERGO hybrid electrode is due to the synergic effect of both components of PANI-HS and ERGO. This effect is mainly due to the following two factors. First, the incorporation of PANI-HS into ERGO greatly improves the double layer capacitance of the hybrids by forming a hollow structure which has a high specific surface area. Second, the pseudocapacitance of PANI-HS in the hybrid is enhanced by the highly conductive network formed by the ERGO component, which favors the redox activity of the PANI component. What is more, the specific capacitance of PANI-HS36@ERGO hybrids is much larger than those reported previously, as listed in Table 1, when considering the same current density.

The rate performance of the PANI-HS36 and PANI-HS36@ERGO hybrids is evaluated by charging/discharging at different current densities, as shown in Figure 6b. The PANI-HS36@ERGO hybrids show an improved rate performance with 73% capacitance maintained as current density increases from 0.5 to 5 A $g^{-1}$, while the PANI-HS36 remains about 60% of its capacity in the same current density range. This is possibly because the high conductivity of PANI-HS36@ERGO hybrids accelerates its charge transfer during the discharging process. Therefore, the wrapping with ERGO can be advantageous in those applications that require high operation voltages owing to their better electrochemical stability across a large voltage range and environmental safety.

The electrochemical impedance spectroscopy (EIS) analysis is a powerful and informative technique to evaluate the properties of conductivity, structure, and charge transport in the film/electrolyte interface. The Nyquist plots of ERGO, PANI-HS36, and PANI-HS36@ERGO hybrid electrodes are displayed in Figure 7. The Nyquist plot of PANI-HS36@ERGO hybrid electrode shows a straight line in the low-frequency region and an unconspicuous arc in the high frequency region. This high frequency loop is related to the electronic resistance inside the electrode materials, and the inconspicuous arc in the high frequency region is probably due to the low Faradaic charge transfer resistances.[57] At low frequency, the hybrid electrodes exhibit a more vertical line than neat PANI, showing a better capacitor behavior.[25] The intersection of the curves at the real axis in the range of high-frequency represents solution resistance ($R_s$).[20] The $R_s$ of


dx.doi.org/10.1021/am4003827 | ACS Appl. Mater. Interfaces 2013, 5, 3382−3391

**Table 1. Comparison of Specific Capacitances of the Reported Graphene-PANI Hybrid Based Electrodes and the Present Work**

| samples | C (F $g^{-1}$) | ref |
|---|---|---|
| polyaniline nanowire arrays/graphene oxide | 555 (0.2 A $g^{-1}$) | 18 |
| graphene/polyaniline nanofiber composites | 480 (0.1 A $g^{-1}$) | 19 |
| graphene nanosheets/polyaniline nanofibers composites | 1130 (5 mV $s^{-1}$) | 20 |
| graphene/polyaniline composite paper | 233 (2 mV $s^{-1}$) | 21 |
| graphene/polyaniline nanofiber composite films | 210 (0.3 A $g^{-1}$) | 22 |
| graphene/polyaniline composite film | 640 (0.1 A $g^{-1}$) | 23 |
| polyaniline grafted reduced graphene oxide | 250 (100 mV $s^{-1}$) | 24 |
| graphene oxide/polyaniline composite | 746 (0.2 A $g^{-1}$) | 25 |
| graphene-polyaniline hybrid papers | 489 (0.4 A $g^{-1}$) | 26 |
| graphene nanosheet/polyaniline composite | 1046 (1 mV $s^{-1}$) | 27 |
| modified graphene/polyaniline nanocomposites | 242 (1.5 A $g^{-1}$) | 28 |
| graphene/polyaniline nanofibers composite paper | 301 (0.5 A $g^{-1}$) | 29 |
| amide group-connected graphene–polyaniline nanofiber hybrid | 369 (1 A $g^{-1}$) | 30 |
| graphene/polyaniline flake composites | 764 (0.1 A $g^{-1}$) | 31 |
| polyaniline coated reduced graphene oxide sheets | 361 (0.3 A $g^{-1}$) | 32 |
| graphene-supported vertically aligned polyaniline nanorods | 497 (0.2 A $g^{-1}$) | 33 |
| graphene oxide-covered polyaniline nanoparticles | 487.2 (0.1 A $g^{-1}$) | 34 |
| nanostructured graphene/polyaniline hybrid | 1126 (1 mV $s^{-1}$) | 35 |
| carboxyl-functionalized graphene oxide–polyaniline composite | 525 (0.3 A $g^{-1}$) | 36 |
| surfactant-stabilized graphene/polyaniline nanofiber composites | 526 (0.2 A $g^{-1}$) | 37 |
| graphene/polyaniline hollow sphere hybrids | 614 (1 A $g^{-1}$) | this work |

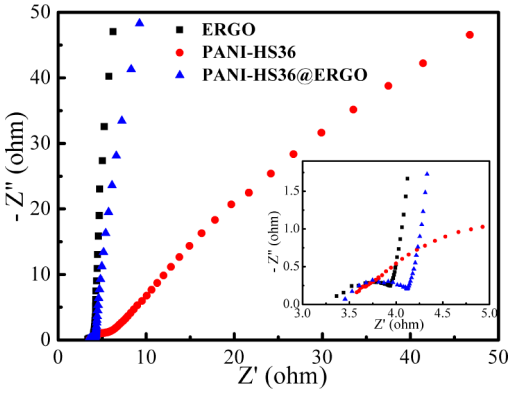


**Figure 7.** Nyquist plots for ERGO, PANI-HS36, and PANI-HS36@ERGO hybrid electrodes. $Z'$, real impedance; $Z''$, imaginary impedance. The inset shows an enlarged scale.

PANI-HS36@ERGO hybrid is about 3.3 Ω, which is smaller than that (3.6 Ω) of PANI. The decrease of $R_s$ may be attributed to the doping process and $\pi-\pi$ stacking between ERGO and PANI-HS36, in which the structure can facilitate the efficient access of electrolyte ions to the electrode surface and shorten the ion diffusion path.

Cycling performance is another key factor in determining the supercapacitor electrodes for many practical applications. Excellent cycling stability is crucial for real supercapacitor operations. The cycling tests for PANI-HS36 and PANI-HS36@ERGO hybrids were carried out under the same current density of 1 A $g^{-1}$, as shown in Figure 8. The typical poor

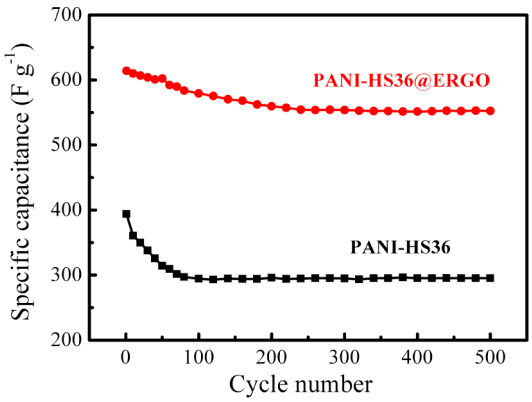


**Figure 8.** Cycling stability of PANI-HS36 and PANI-HS36@ERGO hybrids upon charging–discharging at a current density of 1 A $g^{-1}$.

stability of the specific capacitance during cycling is observed for PANI-HS36. The capacitance of pure PANI-HS36 lost almost 25% (from 394 to 295 F $g^{-1}$) after 500 charging–discharging cycles. During the doping–dedoping process, the PANI-HS36 electrode undergoes swelling, shrinkage, cracking, or breaking that induces gradual deterioration of the conductivity and volumetric changes.[18] The instability of the capacitors based on PANI during long-term charge/discharge cycling is one of their most lethal deficiencies. However, under the same conditions, the capacitance of the PANI-HS36@ERGO hybrids decreased only by 10% (from 614 to 552 F $g^{-1}$). The improved electrochemical stability of the PANI-HS36@ERGO hybrids can be explained as follows. In the hybrid, ERGO sheets act as the frameworks for sustaining PANI-HS, preventing the hollow spheres from severely swelling and shrinking during cycling. Thus, the morphological and electrochemical property changes of PANI-HS induced by charge–discharge cycling are greatly reduced. Therefore, the ERGO sheets could serve dual functions for improving the electrical conductivity and the stability of electrodes, thus greatly enhancing the electrochemical performance and cycling performance.

**3.3. Effect of the Shell Thickness of PANI-HS on Electrochemical Performance.** The shell thickness of PANI-HS can be controlled by changing the amount of aniline monomer. As shown in Figure 2a, when the amount of aniline monomer is halved, the shell thickness of PANI-HS is decreased to about 20 nm. However, some broken spheres were observed with such a thin shell, which is mainly due to the stirring and ultrasonicating during the removal of the PS core. PANI-HS with thicker shell of about 80 nm can be obtained by doubling the amount of aniline monomer, as shown in Figure 2c. Nevertheless, excessive aniline monomer will polymerize itself and some nanofibers can usually be obtained.

The electrochemical performances of PANI-HS with different shell thicknesses were also investigated. The corresponding CV curves at a scan rate of 10 mV $s^{-1}$ and charge–discharge curves at a current density of 1 A $g^{-1}$ are shown in Figure 9. The results show that PANI-HS36 has the largest area of


dx.doi.org/10.1021/am4003827 | ACS Appl. Mater. Interfaces 2013, 5, 3382–3391

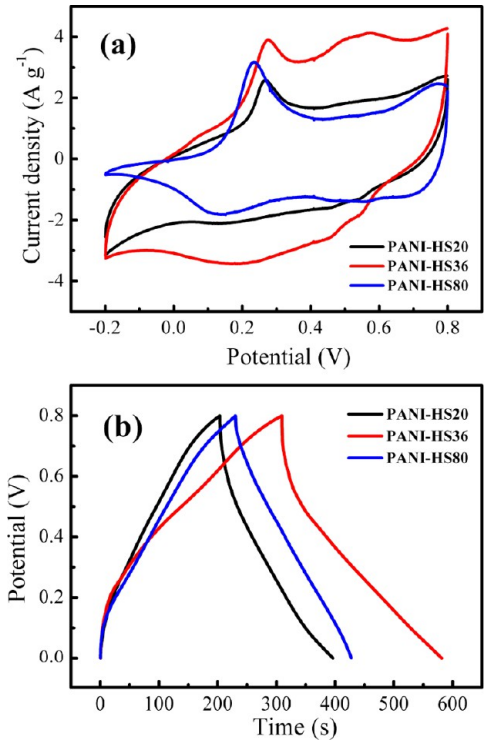


**Figure 9.** (a) CV curves (scan rate 10 mV s$^{-1}$) and (b) galvanostatic charge−discharge curves (at current density of 1 A g$^{-1}$) of PANI-HS with different shell thicknesses.

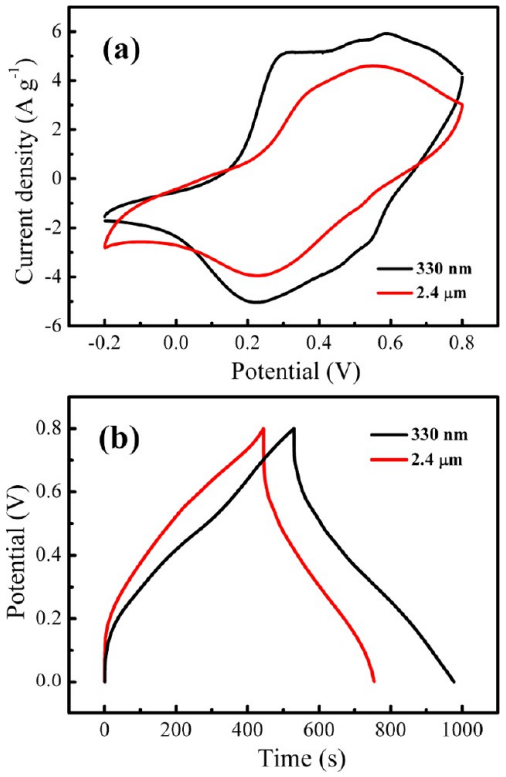


**Figure 10.** (a) CV curves (scan rate 10 mV s$^{-1}$) and (b) galvanostatic charge−discharge curves (at a current density of 1 A g$^{-1}$) of PANI-HS36@ERGO hybrids with different sphere sizes.

surrounded CV loops and the longest discharging duration, indicating an optimized electrochemical performance. The poorer performance of PANI-HS20 is mainly attributed to its broken morphology as indicated in the TEM image (Figure 2a). Some hollow spheres were broken and suppressed into pieces which would reduce the surface area, leading to less electroactive regions for pseudocapacitance. On the other hand, a thicker shell thickness of PANI-HS, e.g., PANI-HS80, will increase the diffusion lengths and diffusion resistance of electrolyte ions in the electrode. Besides, some PANI nanofibers are formed with excess aniline, which will reduce the electrode/electrolyte interface areas. Therefore, the PANI-HS36 with optimized electrochemical performance was chosen for the fabrication of PANI-HS@ERGO hybrids in this work.

**3.4. Effect of the PS Sphere Size on Electrochemical Performance.** PS spheres with different diameters were used as the template for fabricating PANI-HS@ERGO hybrids with the same amount of aniline. The electrochemical performances of PANI-HS@ERGO hybrids with inner diameters of 330 nm and 2.4 $\mu$m were investigated, respectively, and the corresponding CV curves and galvanostatic charge−discharge curves were shown in Figure 10. The specific capacitance of PANI-HS@ERGO hybrids with an inner diameter of 2.4 $\mu$m is estimated to be 465 F g$^{-1}$ from the discharging curve, which is much lower than that of 330 nm (614 F g$^{-1}$). The reduced capacitance is probably due to the reduced surface area, resulting in reduced electroactive regions. In addition, bigger hollow spheres tend to collapse after the PS core was removed, as can be seen from the SEM image in Figure 11b. The morphological changes indicate the instability of the PANI-HS@ERGO hybrid with an inner diameter of 2.4 $\mu$m, which will induce shrinkage or cracking during the charging−discharging process, contributing to poorer electrochemical performance and cycling performance. Therefore, PANI-HS@ERGO hybrids with an inner diameter of 330 nm have higher surface area and morphological stability, which is more suitable for application in supercapacitors with high specific capacitance and enhanced cycling stability.

## 4. CONCLUSIONS

In summary, graphene wrapped PANI-HS hybrids have been prepared by a simple electrostatic interaction induced coassembly of GO and PANI-HS, followed by the electrochemical reduction of GO to ERGO. The hollow structures of PANI-HS by utilizing sulfonated PS spheres as hard templates greatly enhance the specific surface areas, providing high electroactive regions and short diffusion lengths. The introduction of graphene into the hybrids can offer highly conductive pathways by bridging adjacent PANI-HS together, facilitating the kinetics for both charge transfer and ion transport throughout the electrodes. Therefore, the hybrids can greatly reduce the diffusion length, resulting in an improvement of electrochemical properties of the hybrid materials. The PANI-HS36@ERGO hybrids have a high specific capacitance of 614 F g$^{-1}$ at a current density of 1 A g$^{-1}$ in 1 M $H_2SO_4$ solution and show an improved rate performance with 73% capacitance maintained as the current density increases from 0.5 to 5 A g$^{-1}$. Furthermore, the PANI-HS36@ERGO hybrids as electrode materials have a good cycling stability, and the capacitance was maintained at 90% after 500 charging−discharging cycles at a current density of 1 A g$^{-1}$. The greatly enhanced specific capacitance is due to the synergic effect of the two components of ERGO and PANI-HS. The PANI-HS@ERGO hybrids with high specific capacitance and good cycling

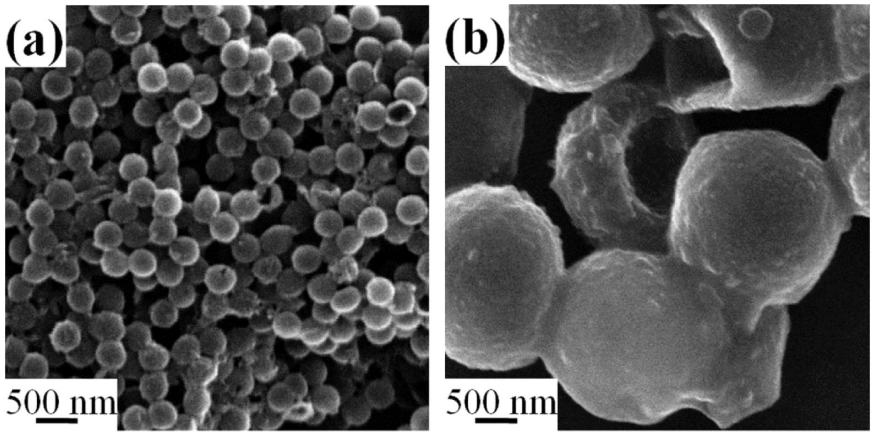


**Figure 11.** SEM images of PANI-HS36@GO hybrids with different sphere sizes of (a) 330 nm and (b) 2.4 μm.

stability are quite suitable and promising electrode materials for high-performance supercapacitors.

## ■ ASSOCIATED CONTENT

### Supporting Information

FTIR spectra of PS and sulfonated PS spheres, $N_2$ adsorption/desorption isotherms of PANI-HS36@GO hybrids, Raman spectra of GO, ERGO, PANI-HS36, PANI-HS36@GO hybrids, and PANI-HS36@ERGO hybrids, and CV curves of PANI-HS36, PANI-HS36@GO hybrids, and PANI-HS36@ERGO hybrids. This material is available free of charge via the Internet at http://pubs.acs.org.

## ■ AUTHOR INFORMATION

### Corresponding Author

*E-mail: txliu@fudan.edu.cn. Phone: +86-21-55664197. Fax: +86-21-65640293.

### Notes

The authors declare no competing financial interest.

## ■ ACKNOWLEDGMENTS

The authors are grateful for the financial support from the National Natural Science Foundation of China (Grant 51125011) and the "Shu Guang" project (Grant 09SG02) supported by Shanghai Municipal Education Commission and Shanghai Education Development Foundation.

## ■ REFERENCES

(1) Huang, Y.; Liang, J. J.; Chen, Y. S. *Small* **2012**, *8*, 1805−1834.
(2) Winter, M.; Brodd, R. J. *Chem. Rev.* **2004**, *104*, 4245−4269.
(3) Stoller, M. D.; Park, S.; Zhu, Y.; An, J.; Ruoff, R. S. *Nano Lett.* **2008**, *8*, 3498−3502.
(4) Yu, G. H.; Hu, L. B.; Vosgueritchian, M.; Wang, H. L.; Xie, X.; McDonough, J. R.; Cui, X.; Cui, Y.; Bao, Z. N. *Nano Lett.* **2011**, *11*, 2905−2911.
(5) Huang, J. S.; Sumpter, B. G.; Meunier, V. *Angew. Chem., Int. Ed.* **2008**, *47*, 520−524.
(6) Aboutalebi, S. H.; Chidembo, A. T.; Salari, M.; Konstantinov, K.; Wexler, D.; Liu, H. K.; Dou, S. X. *Energy Environ. Sci.* **2011**, *4*, 1855−1865.
(7) Lang, J. W.; Yan, X. B.; Yuan, X. Y.; Yang, J.; Xue, Q. J. *J. Power Sources* **2011**, *196*, 10472−10478.
(8) Rakhi, R. B.; Chen, W.; Cha, D.; Alshareef, H. N. *J. Mater. Chem.* **2011**, *21*, 16197−16204.
(9) Mi, H. Y.; Zhang, X. G.; Ye, X. G.; Yang, S. D. *J. Power Sources* **2008**, *176*, 403−409.
(10) Liu, C. G.; Yu, Z. N.; Neff, D.; Zhamu, A.; Jang, B. Z. *Nano Lett.* **2010**, *10*, 4863−4868.
(11) Li, Y. M.; Zijll, M. V.; Chiang, S.; Pan, N. *J. Power Sources* **2011**, *196*, 6003−6006.
(12) Xia, J. L.; Chen, F.; Li, J. H.; Tao, N. J. *Nat. Nanotechnol.* **2009**, *4*, 505−509.
(13) Novoselov, K. S.; Geim, A. K.; Morozov, S. V.; Jiang, D.; Zhang, Y.; Dubonos, S. V.; Grigorieva, I. V.; Firsov, A. A. *Science* **2004**, *306*, 666−669.
(14) Rao, C. N. R.; Sood, A. K.; Subrahmanyam, K. S.; Govindaraj, A. *Angew. Chem., Int. Ed.* **2009**, *48*, 7752−7778.
(15) Zhang, Y. B.; Tan, Y. W.; Stormer, H. L.; Kim, P. *Nature* **2005**, *438*, 201−204.
(16) Huang, X.; Qi, X. Y.; Boey, F.; Zhang, H. *Chem. Soc. Rev.* **2012**, *41*, 666−686.
(17) Pumera, M. *Chem. Soc. Rev.* **2010**, *39*, 4146−4157.
(18) Xu, J. J.; Wang, K.; Zu, S. Z.; Han, B. H.; Wei, Z. X. *ACS Nano* **2010**, *4*, 5019−5026.
(19) Zhang, K.; Zhang, L. L.; Zhao, X. S.; Wu, J. S. *Chem. Mater.* **2010**, *22*, 1392−1401.
(20) Li, J.; Xie, H. Q.; Li, Y.; Liu, J.; Li, Z. X. *J. Power Sources* **2011**, *196*, 10775−10781.
(21) Kumar, N. A.; Choi, H. J.; Shin, Y. R.; Chang, D. W.; Dai, L. M.; Baek, J. B. *ACS Nano* **2012**, *6*, 1715−1723.
(22) Wu, Q.; Xu, Y. X.; Yao, Z. Y.; Liu, A.; Shi, G. Q. *ACS Nano* **2010**, *4*, 1963−1970.
(23) Feng, X. M.; Li, R. M.; Ma, Y. W.; Chen, R. F.; Shi, N. E.; Fan, Q. L.; Huang, W. *Adv. Funct. Mater.* **2011**, *21*, 2989−2996.
(24) Wang, D. W.; Li, F.; Zhao, J. P.; Ren, W. C.; Chen, Z. G.; Tan, J.; Wu, Z. S.; Gentle, I.; Lu, G. Q.; Cheng, H. M. *ACS Nano* **2009**, *3*, 1745−1756.
(25) Wang, H. L.; Hao, Q. L.; Yang, X. J.; Lu, L. D.; Wang, X. *ACS Appl. Mater. Interfaces* **2010**, *2*, 821−828.
(26) Yan, X. B.; Chen, J. T.; Yang, J.; Xue, Q. J.; Miele, P. *ACS Appl. Mater. Interfaces* **2010**, *2*, 2521−2529.
(27) Yan, J.; Wei, T.; Shao, B.; Fan, Z. J.; Qian, W. Z.; Zhang, M. L.; Wei, F. *Carbon* **2010**, *48*, 487−493.
(28) Sahoo, S.; Karthikeyan, G.; Nayak, G. C.; Das, C. K. *Macromol. Res.* **2012**, *20*, 415−421.
(29) Liu, S.; Liu, X. H.; Li, Z. P.; Yang, S. G.; Wang, J. Q. *New J. Chem.* **2011**, *35*, 369−374.
(30) Liu, J. H.; An, J. W.; Zhou, Y. C.; Ma, Y. X.; Li, M. L.; Yu, M.; Li, S. M. *ACS Appl. Mater. Interfaces* **2012**, *4*, 2870−2876.
(31) Chen, F.; Liu, P.; Zhao, Q. Q. *Electrochim. Acta* **2012**, *76*, 62−68.
(32) Zhang, J. T.; Zhao, X. S. *J. Phys. Chem. C* **2012**, *116*, 5420−5426.
(33) Ma, B.; Zhou, X.; Bao, H.; Li, X. W.; Wang, G. C. *J. Power Sources* **2012**, *215*, 36−42.
(34) Sun, J.; Bi, H. *Mater. Lett.* **2012**, *81*, 48−51.

(35) Wang, H. L.; Hao, Q. L.; Yang, X. J.; Lu, L. D.; Wang, X. *Nanoscale* **2010**, *2*, 2164−2170.
(36) Liu, Y.; Deng, R. J.; Wang, Z.; Liu, H. T. *J. Mater. Chem.* **2012**, *22*, 13619−13624.
(37) Mao, L.; Zhang, K.; Chan, H. S. O.; Wu, J. S. *J. Mater. Chem.* **2012**, *22*, 80−85.
(38) Chen, K. W.; Chen, L. B.; Chen, Y. Q.; Bai, H.; Li, L. *J. Mater. Chem.* **2012**, *22*, 20968−20976.
(39) Wang, Y. F.; Yang, X. W.; Qiu, L.; Li, D. *Energy Environ. Sci.* **2013**, *6*, 477−481.
(40) Lai, X. Y.; Halperta, J. E.; Wang, D. *Energy Environ. Sci.* **2012**, *5*, 5604−5618.
(41) Chen, J. S.; Wang, Z. Y.; Dong, X. C.; Chen, P.; Lou, X. W. *Nanoscale* **2011**, *3*, 2158−2161.
(42) Chen, H.; Zhou, S. X.; Chen, M.; Wu, L. M. *J. Mater. Chem.* **2012**, *22*, 25207−25216.
(43) Tang, X. H.; Liu, Z. H.; Zhang, C. X.; Yang, Z. P.; Wang, Z. L. *J. Power Sources* **2009**, *193*, 939−943.
(44) Lei, Z. B.; Chen, Z. W.; Zhao, X. S. *J. Phys. Chem. C* **2010**, *114*, 19867−19874.
(45) Zhang, J. H.; Chen, Z.; Wang, Z. L.; Zhang, W. Y.; Ming, N. B. *Mater. Lett.* **2003**, *57*, 4466−4470.
(46) Hummers, W. S.; Offeman, R. E. *J. Am. Chem. Soc.* **1958**, *80*, 1339−1339.
(47) Yang, Y.; Chu, Y.; Yang, F. Y.; Zhang, Y. P. *Mater. Chem. Phys.* **2005**, *92*, 164−171.
(48) Dai, X. Y.; Zhang, X.; Meng, Y. F.; Shen, P. K. *New Carbon Mater.* **2011**, *26*, 389−395.
(49) Lei, Z. B.; Zhao, M. Y.; Dang, L. Q.; An, L. Z.; Lu, M.; Lo, A. Y.; Yu, N. Y.; Liu, S. B. *J. Mater. Chem.* **2009**, *19*, 5985−5995.
(50) Chaudhari, H. K.; Kelkar, D. S. *Polym. Int.* **1997**, *42*, 380−384.
(51) Guo, H. L.; Wang, X. F.; Qian, Q. Y.; Wang, F. B.; Xia, X. H. *ACS Nano* **2009**, *3*, 2653−2659.
(52) Wang, Z. J.; Zhou, X. Z.; Zhang, J.; Boey, F.; Zhang, H. *J. Phys. Chem. C* **2009**, *113*, 14071−14075.
(53) Stankovich, S.; Dikin, D. A.; Piner, R. D.; Kohlhaas, K. A.; Kleinhammes, A.; Jia, Y. Y.; Wu, Y.; Nguyen, S. T.; Ruoff, R. S. *Carbon* **2007**, *45*, 1558−1565.
(54) Wang, Y. G.; Li, H. Q.; Xia, Y. Y. *Adv. Mater.* **2006**, *18*, 2619−2623.
(55) Tran-Van, F.; Henri, T.; Chevrot, C. *Electrochim. Acta* **2002**, *47*, 2927−2936.
(56) Li, L. X.; Song, H. H.; Zhang, Q. C.; Yao, J. Y.; Chen, X. H. *J. Power Sources* **2009**, *187*, 268−274.
(57) Wang, Y.; Shi, Z. Q.; Huang, Y.; Ma, Y. F.; Wang, C. Y.; Chen, M. M.; Chen, Y. S. *J. Phys. Chem. C* **2009**, *113*, 13103−13107.